Thin Solid Films 519 (2010) 536–540

Contents lists available at ScienceDirect

Thin Solid Films

journal homepage: www.elsevier.com/locate/tsf

Structure and stimulated emission of a high-quality zinc oxide epilayer grown by atomic layer deposition on the sapphire substrate

H.C. Chen [a], M.J. Chen [a,*], T.C. Liu [a], J.R. Yang [a], M. Shiojiri [b]

[a] Department of Materials Science and Engineering, National Taiwan University, No. 1, Sec. 4, Roosevelt Road, Taipei, 10617 Taiwan, ROC
[b] Professor Emeritus of Kyoto Institute of Technology, 1-297 Wakiyama, Kyoto 618-0091, Japan

ARTICLE INFO

Article history:
Received 20 May 2009
Received in revised form 12 May 2010
Accepted 16 July 2010
Available online 23 July 2010

Keywords:
Zinc oxide
Stimulated emission
Epilayer
Atomic layer deposition
Wide band gap semiconductor
Threading dislocation
X-ray diffraction
Transmission electron microscopy

ABSTRACT

A high-quality ZnO epilayer was grown on the (0001) sapphire substrate by atomic layer deposition (ALD) and followed by high-temperature rapid thermal annealing (RTA). The layer-by-layer growth and low deposition temperature of ALD, as well as the RTA treatment, prevent the formation of columnar structures in the ZnO epilayer. A distorted ZnO layer at the ZnO/sapphire interface, which relaxes the misfit in ZnO leads to a low threading dislocation density in the ZnO epilayer. Optically-pumped stimulated emission was achieved with a low-threshold intensity of 153 kW/cm^2 at room temperature. The good crystalline quality and low-threshold stimulated emission indicate that the ALD approach is appropriate for preparing high-quality ZnO epilayers.

1. Introduction

Zinc oxide (ZnO) has attracted considerable attention as a promising material for ultraviolet (UV) photonic devices such as light-emitting diodes and lasers [1–8]. ZnO also has numerous applications in transparent electronics, piezoelectric devices, gas sensors, solar cells, spin electronics, etc. [9]. The large excitonic binding energy (60 meV) of ZnO suggests that it has excellent UV light emission properties. ZnO also has several other advantages: amenability to conventional wet chemical etching, relatively low material costs, long-term stability, environmental friendliness, biocompatibility, and excellent radiation resistance.

Many techniques have been used to grow high-quality ZnO films, including molecular beam epitaxy (MBE) [10–14], metal-organic chemical vapor deposition (MOCVD) [15–18], chemical vapor deposition (CVD) [19,20], pulsed laser deposition (PLD) [21], radio-frequency magnetron sputtering (RFMS) [22–24], and filtered cathodic vacuum arc technique [25,26]. Lim et al. reported that ZnO films grown on the (0001) sapphire (c-Al_2O_3) at 200–275 °C by electron cyclotron resonance-assisted MBE were basically single crystals, which comprised subgrains with 15–150 nm in size and accompanied by threading dislocations [12]. Generally, a lot of columnar grains were embedded in the ZnO films grown by MOCVD [15–18]. PLD and RFMS may be the most popular techniques for preparation of ZnO films, but they usually require a high growth temperature (above 350 °C or more).

Atomic layer deposition (ALD) is another noteworthy method of growing high-quality ZnO films [27–29]. Unlike the other methods such as CVD, ALD proceeds the reactions solely on the surface of the substrate, leading to self-limiting and layer-by-layer growth. ALD offers many advantages, including easy and accurate thickness control, excellent conformality, high uniformity over a large area, good reproducibility, low defect density, pinhole-free structures, and low deposition temperatures. Recently, Wójcik et al. have examined how to control the preferred orientation of polycrystalline ZnO thin films grown by ALD on the c-Al_2O_3, lime glass, and (001) and (111) Si substrates at 230–400 °C [30]. They have also reported that the ALD ZnO thin films grown on Si substrates at a low temperatures (90–200 °C) are high-quality polycrystalline with a surface roughness of 1–4 nm [31,32]. In this paper, we demonstrate a high-quality ZnO epilayer grown on the c-Al_2O_3 substrate using the ALD technique, followed by high-temperature rapid thermal annealing (RTA). The resulting ZnO film exhibited optically-pumped stimulated emission with a low-threshold intensity, which is consistent with the high crystalline quality revealed by X-ray diffraction (XRD) and transmission electron microscopy (TEM).

* Corresponding author.
E-mail address: mjchen@ntu.edu.tw (M.J. Chen).

0040-6090/$ – see front matter © 2010 Elsevier B.V. All rights reserved.
doi:10.1016/j.tsf.2010.07.069

2. Experiments

A ZnO epilayer was deposited on the c-Al_2O_3 substrate (2 in in diameter) at a low deposition temperature of 180 °C by ALD. We used a Cambridge NanoTech Savannah 100 ALD system, with a reactor chamber of 4 in in diameter and 5 mm in height. Two precursors, Zn $(C_2H_5)_2$ (diethylzinc, DEZn) and H_2O vapor, were carried in by a N_2 flow. The following reactions proceed on the surface:

$$(A)\text{Surface} - \text{OH} + \text{Zn}(C_2H_5)_2 \rightarrow \text{Surface} - \text{O} - \text{Zn} - C_2H_5 + C_2H_6\uparrow$$

$$(B)\text{Surface} - \text{O} - \text{Zn} - C_2H_5 + H_2O \rightarrow \text{ZnO} + \text{Surface} - \text{OH} + C_2H_6\uparrow.$$

The ALD process consisted of a number of identical cycles and repeated the reactions in an ABAB… sequence. Each ALD cycle contained the following sequence: (A) Pulsing time of DEZn was 0.01 s, followed by N_2 purge for 5 s, and (B) Pulsing time of H_2O was 0.1 s, followed by N_2 purge for 5 s. These precursor pulse duration and purging time were set as the most appropriate condition for ZnO deposition in the ALD system used in this experiment. Each ALD cycle deposited ~0.18 nm of ZnO. After deposition, the films were treated by RTA at 950 °C for 5 min in a nitrogen atmosphere to improve the crystal quality.

The crystalline structure of the ZnO epilayer was characterized by XRD and TEM. A PANalytical X'Pert PRO diffractometer with a wavelength of 1.54 Å was used for the XRD measurement. TEM images were recorded using a Tecnai 30 electron microscope equipped with a lens of $Cs = 1.2$ mm and operated at 300 keV. The specimens for TEM observation were prepared by mechanical polishing and ion milling with a Gatan Precision Ion Polish System Model-691. Photoluminescence (PL) spectra were measured in a standard backscattering configuration by collecting the light emission from the top surface of the sample. A continuous wave He–Cd laser ($\lambda = 325$ nm) and a pulsed Nd-YAG laser ($\lambda = 266$ nm, 10 ns pulse width, 15 Hz repetition rate) were used as the excitation sources to measure the spontaneous emission and stimulated emission of the ZnO epilayer at room temperature.

3. Results and discussion

Fig. 1 shows the XRD pattern of the ZnO epilayer, indicating that it was preferentially oriented with respect to the c-Al_2O_3 substrate with the relation of (0001)ZnO//(0001)Al_2O_3. The XRD θ-2θ scan (the inset of Fig. 1) exhibited a sharp ZnO (0002) peak with a full-width at half-maximum (FWHM) of 0.06°. This reveals high crystallinity with the c-axis orientation of the ZnO epilayer.

Fig. 2 shows a cross-sectional TEM image of the ZnO epilayer about 830 nm thick on the c-Al_2O_3 substrate. The highest ZnO growth rate along the c-axis usually results in a columnar morphology in ZnO [11–18]. However, the columnar structures were not observed in the ZnO epilayer grown by ALD and followed by the RTA treatment. This is attributable to the layer-by-layer growth and the low deposition temperature of 180 °C in ALD. The RTA treatment recrystallized the granular particles with strained lattices in the as-deposited ZnO film to a highly crystalline single crystal with the preferred c-axis orientation. The as-deposited ZnO films grown on the c-Al_2O_3 substrate at 180 °C by ALD were composed of granular particles with an average size as small as ~34 nm, which was estimated from X-ray diffraction (0002) peak (with a FWHM width of 0.245°) using Scherrer's equation in our previous experiment [33].

Fig. 3 displays a high-resolution (HR) TEM mage of an area including the ZnO and c-Al_2O_3 substrate. Insets present the computer diffractograms (fast Fourier transform images) a, b, c and all of the areas indicated by a, b, and c and of the whole area in the HRTEM image, respectively. Diffractogram c reveals that ZnO is oriented with the [0$\bar{1}$10] axis parallel to the incident beam and the [0001] axis normal to the film surface. The interfacial area b exhibiting brighter contrast can be also identified as the ZnO crystal with almost the same orientation with the crystal in c. The difference in contrast between c and b might be caused by a very small difference in the diffraction condition. Thus, the dark area c and the bright area b are almost similar in the crystal structure, although they are not the same because the lattices of the interfacial area b are more distorted under the influence of the c-Al_2O_3 substrate lattice as seen in the HRTEM image. The Al_2O_3 crystal including the area a is nearly oriented with the [2$\bar{1}$10] axis parallel to the incident beam and the [0001] axis normal to the film surface, which indicates that the ZnO crystal was grown in the epitaxial relation with respect to the c-Al_2O_3: [0001] ZnO//[0001]Al_2O_3 and [0$\bar{1}$10]ZnO// [2$\bar{1}$10]Al_2O_3. The lattice of ZnO crystal in the interfacial area is conjugated rather homogeneously and coherently with the lattice of the c-Al_2O_3 crystal, with very few threading dislocations (also see Fig. 2). It should be noted that the threading dislocations used to occur in the ZnO crystals grown by other methods due to a lattice misfit as large as 18% between ZnO and c-Al_2O_3 [12]. The ZnO grown on c-Al_2O_3 by ALD might relax the misfit by distorting its lattice in the interfacial layer. Consequently, the ZnO crystal developed to the single crystal as seen in Fig. 2, in a short

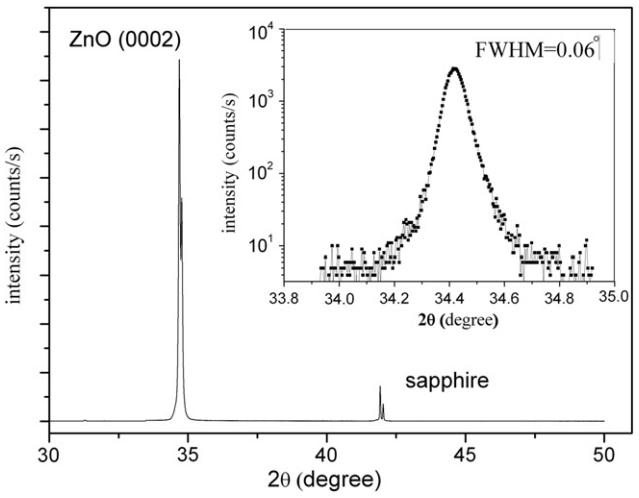

Fig. 1. X-ray diffraction pattern of the ZnO epilayer grown on the c-Al_2O_3 substrate by ALD and treated by post-deposition RTA.

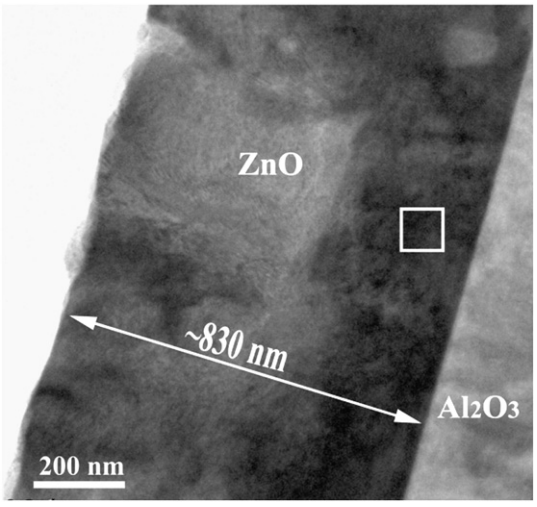

Fig. 2. Cross-sectional transmission electron microscopy (TEM) image of the ZnO epilayer grown on the c-Al_2O_3 substrate by ALD and treated by post-deposition RTA.

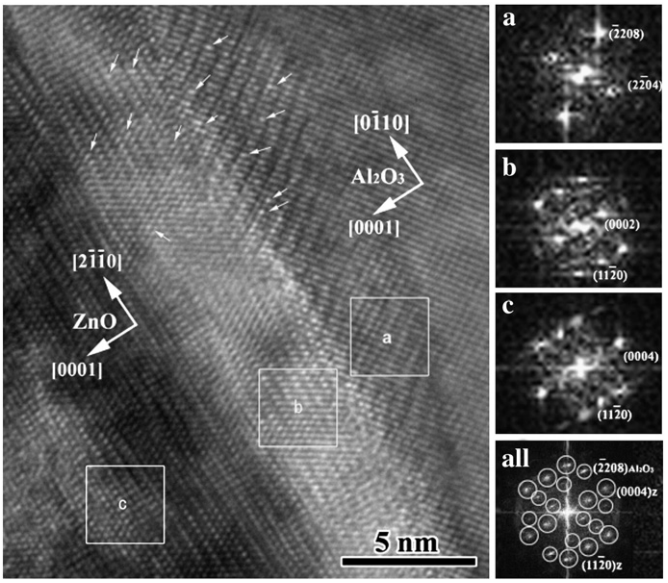

Fig. 3. High-resolution TEM (HRTEM) image of an area including the ZnO/Al_2O_3 interface. Computer diffractograms are of the small areas indicated by a, b, and c and the whole area (all). Indexes in diffractogam a correspond to the lattice fringes of the Al_2O_3 crystal and indexes in diffractograms b and c correspond to the lattice fringes of the ZnO crystal. In the diffractogram all, the spots enclosed by large circles come from ZnO and the spots enclosed by small circles originate from Al_2O_3.

annealing time of 5 min. Fig. 4 shows an HR-TEM image of the ZnO epilayer, whose area is indicated by the square in Fig. 2. The image reveals that the crystal is a nearly perfect ZnO crystal although some lattice distortion still appears as the traces of coalescence growth between the granular particles in the as-deposited ZnO film.

The spots in the diffractogaram of the whole area in Fig. 3, all, can be indexed as the spots form the ZnO and Al_2O_3 lattice fringes. We cannot recognize any other crystal in our specimen although Wang et al. identified the Al_2ZnO_4 phase in a TEM image at the interface between ZnO and Al_2O_3 [21]. The Al_2ZnO_4 phase might be formed by the reaction of ZnO and Al_2O_3 during PLD at a high growth temperature of 600 °C and a long annealing treatment at 900 °C for 2 h. In this study, the ALD growth temperature was as low as 180 °C and post-deposition annealing treatment was short (950 °C for 5 min). However, we can see extraordinarily bright spots (some examples of which are indicated by arrowheads in Fig. 3) in the lattice fringes in the HRTEM image, which may be ascribed to the substituted Al atoms in the interfacial ZnO layer and the Al vacancies in the Al_2O_3 crystal near the interface. Therefore, it is reasonable to assume that the Al atoms might diffuse from the substrate to the ZnO crystal during the RTA treatment.

The high crystallinity shown in the XRD and TEM measurements suggests good light emission properties of the ZnO epilayer grown by ALD. Fig. 5 shows the spontaneous emission PL spectrum of the ZnO epilayer at room temperature. The PL spectrum exhibited a strong near-band-edge (NBE) emission at 3.28 eV, nearly free of the defect-related band. The inset in Fig. 5 presents the same PL spectrum in the logarithm scale, indicating a very weak defect-related band at 2.57 eV associated with the oxygen vacancy (V_O) [8]. It can be observed that the intensity of the NBE emission (3.28 eV) is about two orders of magnitude larger than that of the defect-related band (2.57 eV).

Fig. 6 shows the stimulated emission PL spectra of the ZnO epilayer at various excitation intensities from 14.9 to 339.5 kW/cm^2. At a low excitation intensity, the spectral peak located around 3.26 eV, ascribed to the radiative recombination of free excitons [34]. A spectral peak appeared at 3.17 eV as the excitation intensity increased. This spectral peak comes from the radiative recombination associated with exciton–exciton scattering, in which one exciton recombines to emit a photon with the energy given by [35]

$$E_n = E_{ex} - E_B^{ex}\left(1-\frac{1}{n^2}\right) - \frac{3}{2}k_BT \quad (1)$$

and the other exciton is scattered to a higher energy state ($n>2$). In Eq. (1), E_{ex} is the free-exciton energy, E_B^{ex} is the binding energy of the exciton (60 meV) [36], n is the quantum number of the excited exciton, and k_BT is thermal energy. The difference between E_{ex} and E_n ($n>>2$) as calculated by Eq. (1) is 99 meV, which is in good agreement with the experimental results. Further increase in the excitation intensity shifted the spectral peak from 3.16 eV to 3.12 eV, which is attributable to the radiative recombination from the electron-hole plasma (EHP). The EHP was formed when the exciton concentration exceeded the Mott density, which was estimated by Klingshirn et al. to be [37]

$$n_M^{ZnO} \approx 3\times 10^{17}\ cm^{-3}. \quad (2)$$

In the present study, the exciton concentration n_p can be estimated using the following expression [36]:

$$n_p = \frac{I_{exc}\tau}{\hbar\omega_{exc}d} \quad (3)$$

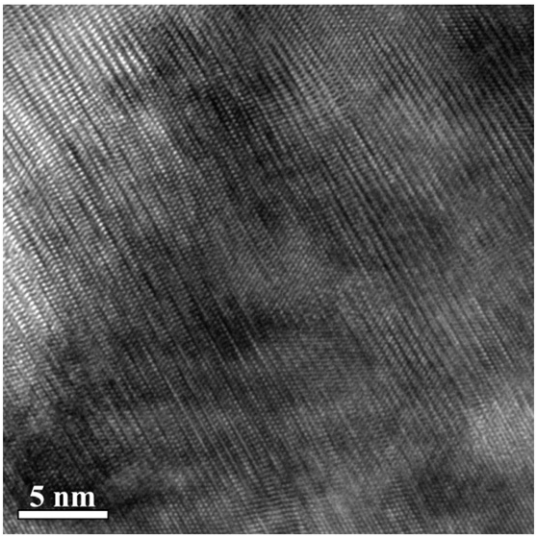

Fig. 4. HRTEM image of the ZnO epilayer enclosed by a square in Fig. 2.

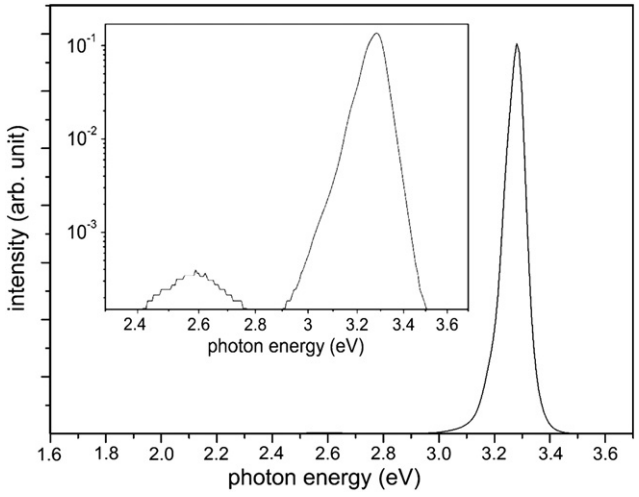

Fig. 5. Spontaneous emission PL spectrum of the ZnO epilayer (grown on the c-Al_2O_3 substrate by ALD and treated by post-deposition RTA), pumped by a CW He–Cd laser at room temperature. The inset is the plot of the same PL spectrum in the logarithm scale.

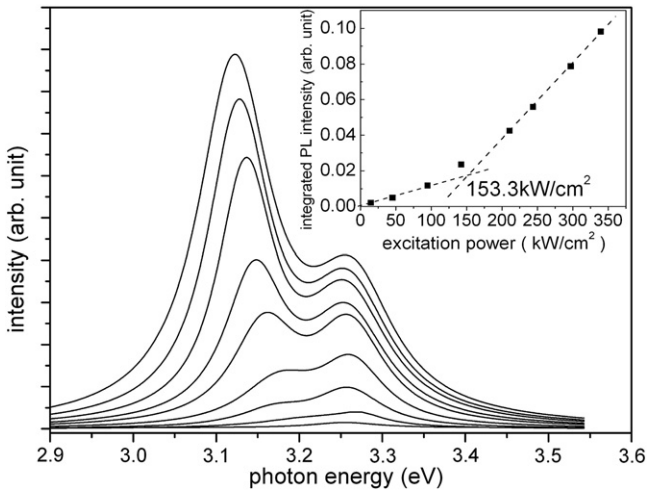

Fig. 6. Stimulated emission PL spectrum of the ZnO epilayer (grown on the *c*-Al_2O_3 substrate by ALD and treated by post-deposition RTA), pumped by a pulsed Nd-YAG laser at room temperature. The inset shows the characteristic of the integrated PL intensity *vs.* the excitation intensity.

where I_{exc} and $\hbar\omega_{exc}$ are the optical intensity and photon energy of the pumping laser beam, d denotes the film thickness, and τ is the lifetime of the exciton with a typical value of about 300 ps [38]. According to Eq. (3), the exciton concentration at the excitation intensity of 210.9 kW/cm^2 is about 1.03×10^{18} cm^{-3}, which is higher than the Mott density given by Eq. (2). A further increase in the excitation intensity causes an increase in the EHP concentration, leading to a reduction in the ZnO bandgap energy as a result of bandgap renormalization [39]. Therefore, a continuous red-shift of the spectral peak associated with EHP from 3.16 eV to 3.12 eV was observed as the excitation intensity increased.

The inset of Fig. 6 plots the curve of integrated PL intensity *vs.* excitation intensity, showing a rapid increase as the excitation intensity is greater than a threshold value of 153 kW/cm^2. The significant increase in the PL intensity for the excitation intensity greater than the threshold and the appearance of the spectral peaks demonstrate the stimulated emission from the ZnO epilayer. Note that such a stimulated emission was not observed in the as-deposited ZnO films [33], indicating that the post-deposition RTA treatment greatly improves the crystal quality to achieve the low-threshold stimulated emission in ZnO. Since the diameter of the focused pumping laser beam in the PL measurement was about 1 mm, which is much greater than the film thickness, it is likely that the stimulated emission resulted from the closed loop paths in the direction parallel to the film surface. The scattering of the photons propagating in the in-plane direction by the optical scattering centers and crystalline grains leads to the observation of stimulated emission in the direction perpendicular to the film surface [34]. It is worthy of mention that the threshold intensity for optically-pumped stimulated emission of this ZnO epilayer is much smaller than that of GaN (800 kW/cm^2) [40,41], suggesting the high optical quality of the ZnO epilayer grown by ALD. In addition, the ZnO epilayer has a large-area uniformity and good reproducibility owing to the benefits of ALD, indicating that the ALD technique is applicable to the preparation of high-quality ZnO epilayers.

4. Summary

This study presents the structure and low-threshold stimulated emission of the ZnO epilayer grown on *c*-Al_2O_3 by ALD and treated by the post-deposition RTA process. The XRD measurement indicates that the ZnO epilayer was highly *c*-axis orientated. The cross-sectional TEM images show that the columnar structures were not formed in the ZnO epilayer, which may be attributed to the layer-by-layer growth and low deposition temperature of ALD, together with the coalescence or recrystallization between the deposited granular particles during the RTA process. The HRTEM images display that a distorted ZnO layer exists at the ZnO/sapphire interface. Because of the relaxation of the misfit by the interfacial distorted layer coupled with the layer-by-layer growth of ALD, no obvious threading dislocations appeared in the TEM images even though the lattice mismatch between ZnO and *c*-Al_2O_3 is up to 18%. A dominant UV emission at 3.28 eV with a negligible defect band was shown in the spontaneous emission PL spectrum. Optically-pumped stimulated emission associated with the exciton–exciton scattering and EHP was observed with a low threshold of 153 kW/cm^2 at room temperature. The negligible defect-related emission and low-threshold stimulated emission are ascribed to the good crystalline quality of the ZnO epilayer, indicating that the ZnO epilayers grown by the ALD technique are applicable to next-generation UV photonic devices. The low threading dislocation density also suggests that the ZnO grown by ALD is a suitable buffer layer for GaN epitaxy for future investigation.

References

[1] A. Tsukazaki, A. Ohtomo, T. Onuma, M. Ohtani, T. Makino, M. Sumiya, K. Ohtani, S.F. Chichibu, S. Fuke, Y. Segawa, H. Ohno, H. Koinuma, M. Kawasaki, Nat. Mater. 4 (2005) 42.
[2] X.Li. Guo, J.H. Choi, H. Tabata, T. Kawai, Jpn. J. Appl. Phys. 40 (2001) L177.
[3] J.A. Lubguban, H.W. White, B.J. Kim, Y.S. Park, C.J. Youn, Appl. Phys. Lett. 88 (2006) 241108.
[4] W.Z. Xu, Z.Z. Ye, Y.J. Zeng, L.P. Zhu, B.H. Zhao, L. Jiang, J.G. Lu, H.P. He, Appl. Phys. Lett. 88 (2006) 173506.
[5] S.J. Jiao, Z.Z. Zhang, Y.M. Lu, D.Z. Shen, B. Yao, J.Y. Zhang, B.H. Li, D.X. Zhao, X.W. Fan, Z.K. Tang, Appl. Phys. Lett. 88 (2006) 031911.
[6] Ya.I. Alivov, E.V. Kalinina, A.E. Cherenkov, D.C. Look, B.M. Ataev, A.K. Omaev, M.V. Chukichev, D.M. Bagnall, Appl. Phys. Lett. 83 (2003) 4719.
[7] D.C. Look, Mater. Sci. Eng. B 80 (2001) 383.
[8] U. Ozgur, Ya.I. Alivov, C. Liu, A. Teke, M.A. Reshchikov, S. Dogan, V. Avrutin, S.J. Cho, H. Morkocd, J. Appl. Phys. 98 (2005) 041301.
[9] C. Jagadish, S.J. Pearton, Zinc Oxide Bulk, Thin Films and Nanostructures: Processing, Properties and Application, Elsevier, Oxford, 2006.
[10] Y. Chen, D. Bagnall, T. Yao, Mater. Sci. Eng. B 75 (2000) 190.
[11] J.M. Yuk, J.Y. Lee, J.H. Jung, T.W. Kim, D.I. Son, W.K. Choi, Appl. Phys. Lett. 90 (2007) 031907.
[12] S.H. Lim, D. Shindo, H.B. Kang, K. Nakamura, J. Vac. Sci. Technol. B 19 (2) (2001) 506.
[13] A. Setiawan, Z. Vashaei, M.W. Cho, T. Yao, H. Kato, M. Sano, K. Miyamoto, I. Yonenaga, H.J. Ko, J. Appl. Phys. 96 (2004) 3763.
[14] S.H. Lim, J. Washburn, Z.L. Weber, D. Shindo, J. Vac. Sci. Technol. A 19 (2001) 2601.
[15] V. Sallet, C. Thiandoume, J.F. Rommeluere, A. Lusson, A. Riviere, J.P. Riviere, O. Gorochov, R. Triboulet, V.M. Sanjose, Mater. Lett. 53 (2002) 126.
[16] C.M. Hou, K.K. Huang, Z.M. Gao, X.S. Li, S.H. Feng, Y.T. Zhang, G.T. Du, Chem. Res. Chinese. U. 22 (2006) 552.
[17] C.Y. Liu, B.P. Zhang, N.T. Binh, Y. Segawa, Appl. Phys. B 79 (2004) 83.
[18] W.Y. Shiao, C.Y. Chi, S.C. Chin, C.F. Huang, T.Y. Tang, Y.C. Lu, Y.L. Lin, L. Hong, F.Y. Jen, C.C. Yang, B.P. Zhang, Y. Segawa, J. Appl. Phys. 99 (2006) 054301.
[19] J. Hu, R.G. Gordon, J. Appl. Phys. 71 (1992) 880.
[20] K. Minegishi, Y. Koiwai, Y. Kikuchi, K. Yano, M. Kasuga, A. Shimizu, Jpn. J. Appl. Phys. 36 (1997) L1453.
[21] Y.G. Wang, N. Ohashi, Y. Wada, I. Sakaguchi, T. Ohgaki, H. Haneda, J. Appl. Phys. 100 (2006) 023524.
[22] P.F. Carcia, R.S. McLean, M.H. Reilly, G. Nunes, Appl. Phys. Lett. 82 (2003) 1117.
[23] L.Y. Chen, W.H. Chen, J.J. Wang, F.C.N. Hong, Y.K. Su, Appl. Phys. Lett. 85 (2004) 5628.
[24] H.H. Hsieh, C.C. Wu, Appl. Phys. Lett. 89 (2006) 041109.
[25] C. Yuen, S.F. Yu, E.S.P. Leong, H.Y. Yang, S.P. Lau, H.H. Hng, IEEE J. Quantum Electron. 41 (2005) 970.
[26] Y.G. Wang, S.P. Lau, H.W. Lee, S.F. Yu, B.K. Tay, X.H. Zhang, K.Y. Tse, H.H. Hng, J. Appl. Phys. 94 (2003) 1597.
[27] M. Ritala, M. Leskela, Nanotechnology 10 (1999) 19.
[28] L. Niinisto, J. Paivasaari, J. Niinisto, M. Putkonen, M. Nieminen, Phys. Stat. Sol. (a) 201 (2004) 1443.
[29] J. Lim, K. Shin, H.W. Kim, C. Lee, J. Lumin. 109 (2004) 181.
[30] A. Wojcik, M. Godlewski, E. Guziewicz, R. Minikayev, W. Paszkowicz, J. Cryst. Growth 310 (2008) 284.
[31] E. Guziewicz, I.A. Kowalik, M. Godlewski, K. Kopalko, V. Osinniy, A. Wojcik, S. Yatsunenko, E. Usakowska, W. Paszkowicz, M. Guziewicz, J. Appl. Phys. 103 (2008) 033515.
[32] I.A. Kowalik, E. Guziewicz, K. Kopalko, S. Yatsunenko, M. Godlewski, A. Wojcik, Acta Phys. Pol. A 112 (2007) 401.

[33] H.C. Chen, M.J. Chen, M.K. Wu, Y.C. Cheng, F.Y. Tsai, IEEE J. Sel. Top. Quantum Electron. 14 (2008) 1053.
[34] X.Q. Zhang, I. Suemune, H. Kumano, J. Wang, S.H. Huang, J. Appl. Phys. 96 (2004) 3733.
[35] C. Klingshirn, Phys. Status Solidi B 71 (1975) 547.
[36] D.C. Reynolds, D.C. Look, B. Jogai, C.W. Litton, G. Cantwell, W.C. Harsch, Phys. Rev. B. 60 (1999) 2340.
[37] C. Klingshirn, R. Hauschild, J. Fallert, H. Kalt, Phys. Rev. B 75 (2007) 115203.
[38] M.H. Huang, S. Mao, H. Feick, H. Yan, Y. Wu, H. Kind, E. Weber, R. Russo, P. Yang, Science 292 (2001) 1897.
[39] P. Zu, Z.K. Tang, G.K.L. Wong, M. Kawasaki, A. Ohtomo, H. Koinuma, Y. Segawa, Solid State Commun. 103 (1997) 459.
[40] X.H. Zhang, T.J. Schmidt, W. Shan, J.J. Song, B. Goldenberg, Appl. Phys. Lett. 66 (1995) 1.
[41] D. Wiesmann, I. Brener, L. Pfeiffer, M.A. Khan, C.J. Sun, Appl. Phys. Lett. 69 (1996) 3384.